Isolated core excitation of high-orbital-quantum-number Rydberg states of ytterbium

Henri Lehec ⬡,[*] Xin Hua ⬡,[†] Pierre Pillet, and Patrick Cheinet ⬡[‡]

Laboratoire Aimé Cotton, CNRS, Univ. Paris-Sud, Université Paris-Saclay, Bât. 505, 91405 Orsay, France

We study isolated core excitation of ultracold ytterbium Rydberg atoms of high orbital angular momentum quantum number ℓ. Measurements were performed on the $6s_{1/2}40\ell \rightarrow 6p_{1/2}40\ell$ transition with $\ell = 5$–9. The extracted energy shifts and autoionization rates are in good agreement with a model based on independent electrons, taking interactions into account in a perturbative approach. We reveal a slow decrease in the autoionization rates with ℓ, explained by the strong coupling of the $6p_{1/2}n\ell$ autoionizing state with the $5d_{3/2}\epsilon\ell'$ continua compared to previously studied divalent atoms.

I. INTRODUCTION

Rydberg atoms offer an ideal platform for quantum simulation experiments [1]. Thanks to their strong, long-range and tunable interactions, they are good candidates to study many-body phenomena. Atoms trapped in optical lattices have been used to demonstrate spatial correlations in the Rydberg excitation [2] and more recently, tunable arrays of Rydberg atoms have been used to demonstrate the simulation of Ising spin systems [3,4] and topological matter [5]. In these experiments, the imaging technique relies on the fluorescence of the atoms after returning them to their ground state. A drawback of this technique is the false-positive detection of residual nonevacuated ground state atoms. This typically sets a limit on the maximum number of atoms to a few hundred, which is a severe limitation for future quantum simulation experiments.

We investigate here the possibility of imaging the Rydberg atoms through the fluorescence induced by isolated core excitation (ICE) [6]. Possible in multivalent atoms such as strontium, barium, ytterbium, etc., this technique could allow efficient and accurate *in situ* imaging of the Rydberg atoms. However, due to the interaction between the two valence electrons, doubly excited Rydberg atoms may rapidly autoionize [7,8]. A first method to reduce autoionization is to use high-principal-quantum-number states [6,9]. The autoionization rate is known to evolve as $1/n^3$, following the Rydberg wave function amplitude evolution close to the core. Another method is to use the strong centrifugal barrier of high ℓ states that prevents the Rydberg electron from interacting with the ionic core. In both barium [10] and strontium [6] doubly excited high ℓ states' autoionization rates exhibit a $10^{-\ell}$ dependence, but unlike the evolution with n, this law is not universal and cannot be demonstrated theoretically.

In this article, we study the ICE $6s_{1/2}40\ell \rightarrow 6p_{1/2}40\ell$ for high $\ell = 5$–9 Rydberg states of ^{174}Yb under ultracold conditions. We show good agreement between our measurements and a simple theoretical model based on independent electrons, where interactions are treated perturbatively. In ytterbium, the coupling of the $6p_{1/2}n\ell$ autoionizing state with the $5d_{3/2}\epsilon\ell'$ continua is particularly strong, with the result that the autoionization rate decrease with ℓ is relatively weak, compared to that of barium or strontium.

II. EXPERIMENTAL METHODS

The schematic of the experiment is represented in Fig. 1. Cold ^{174}Yb atoms are continuously loaded in a three-dimensional magneto-optical trap operating on the intercombination line $6s^2\ ^1S_0 \rightarrow 6s6p\ ^3P_1$ at 555.8 nm. The atomic cloud contains about 1×10^6 atoms and has a size of about 1 mm. In order to selectively excite the $6sn\ell$ state with high-orbital quantum number ℓ, we use the so-called *Stark-switching* technique [11]. The Rydberg excitation is performed with two photons through the intermediate $6s6p\ ^1P_1$ level. This first level is reached using an external cavity diode laser (ECDL) locked on the $6s^2\ ^1S_0 \rightarrow 6s6p\ ^1P_1$ resonance (λ_1), collimated to a 1 mm waist and with a peak intensity of about 30 mW/cm^2 on the atoms. The second photon is provided by a cavity doubled titanium-sapphire laser at around 395 nm (λ_2) with a waist of about 0.5 mm and a peak intensity of 50 W/cm^2. Both lasers are pulsed on simultaneously during 5 μs.

The two-photon excitation is performed in the presence of a static electric field in order to allow the excitation of states connecting to the different $6s40\ell$ levels, as can be seen in Fig. 2. The states appear as groups of two or three peaks and we choose to excite the atoms at the strongest peak for each group. Computation of the exact Stark structure of a divalent atom has not been performed yet, which prevents predicting the fine details of the zero-field state to which a Stark state is connected. Nevertheless, it has been demonstrated that they adiabatically connect to states of known orbital momentum [11]. The electric field is then ramped down with a

---

[*]Present address: Institut für Physik, Univ. Mainz, Staudingerweg 7, 55128 Mainz, Germany; hlehec@uni-mainz.de

[†]Present address: Institut de Physique de Nice (INPHYNI), Parc Valrose, 06108 Nice, France; xin.hua@unice.fr

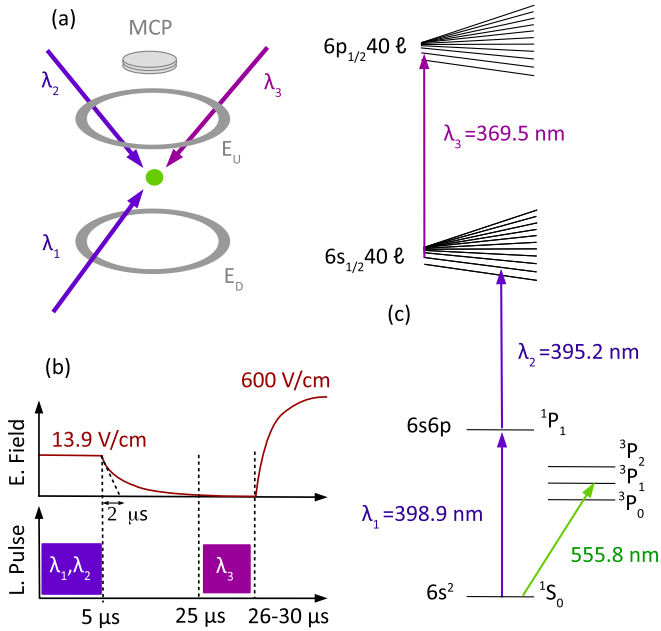[‡]Corresponding author: patrick.cheinet@u-psud.fr

FIG. 1. (a) Schematic of the experimental setup. (b) Time sequence of the experiment. A cold cloud of ytterbium atoms is laser excited ($\lambda_1 + \lambda_2$) to a high-ℓ Rydberg state in the presence of a static electric field (provided by electrode E_U). After the adiabatic ramp-down of the electric field, a third laser λ_3 is applied to excite the isolated core transition. Resulting autoionized atoms are guided towards an MCP detector by a pulse applied to electrode E_D. (c) Scheme of energy levels involved in this experiment.

$2\,\mu$s time constant to minimize diabatic transfers to adjacent $6s40\ell \pm 1$ states. The total ramp-down time of $20\,\mu$s is chosen shorter than the Rydberg levels total lifetime. In order to avoid unwanted residual Stark mixing of the $6s40\ell$ states at the end of the ramp, eight electrodes are used to null stray electric fields to below 10 mV/cm.
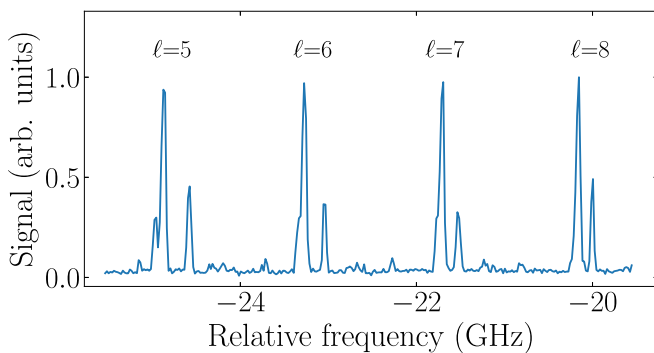

FIG. 2. Rydberg excitation spectrum of the states connecting to $n = 40$, $\ell = 5$ to $\ell = 8$ levels in the presence of a static electric field of 13.9 V/cm . Frequencies are given relatively to the center of the $n = 40$ multiplicity. The ℓ labels correspond to the zero-field ℓ states to which the Stark states are adiabatically connected. For the lowest ℓ states a substructure of three peaks can be seen. For every ℓ state, the strongest peak was excited.

Afterwards, isolated core excitation is performed on the $6s_{1/2}40\ell \rightarrow 6p_{1/2}40\ell$ transition at 369.5 nm (λ_3) using an ECDL laser which is pulsed on with a variable duration of 1–5 μs with an Acousto-Optic Modulator (AOM). The durations were chosen to produce a significant autoionization signal, without depleting the Rydberg cloud. The intensity on the atoms is around 10 mW/cm^2 and the wavelength is measured thanks to a calibrated wavemeter (High-Finesse WSU) providing an accuracy of 10 MHz. An electric field ramp is then applied on the E_D electrode in order to guide ions resulting from autoionization towards a microchannel plate (MCP) detector to be estimated as N_{ai} with a gated integrator. After around 2 μs, the electric field reaches the ionization threshold of the Rydberg levels. The resulting ions are subsequently guided to the same detector and arrive at a different time, allowing us to determine the number of residual Rydberg atoms and thus the total number of atoms initially excited to the $6s_{1/2}40\ell$ Rydberg state (N_{tot}).

III. EXPERIMENTAL RESULTS AND ANALYSIS METHOD

In Fig. 3 is plotted the measured ratio of autoionized atoms $R_{ai} = N_{ai}/N_{\text{tot}}$ against the detuning from the $6s_{1/2} \rightarrow 6p_{1/2}$ transition of the bare ^{174}Yb$^+$ ion. Its frequency can be found in [12] and more recently in [13] which provides the value we used of 811.291 500(40) THz for ^{174}Yb. As expected, we notice a decrease of the autoionization linewidth and of the overall shift compared to the bare ion core (IC) transition with ℓ. This is a clear signature of the decreasing influence of the Yb$^+$ ionic core. Finally, we notice an asymmetry of the spectra for the higher ℓ states. We will first discuss the origin of the asymmetry by an analysis of the spectra.
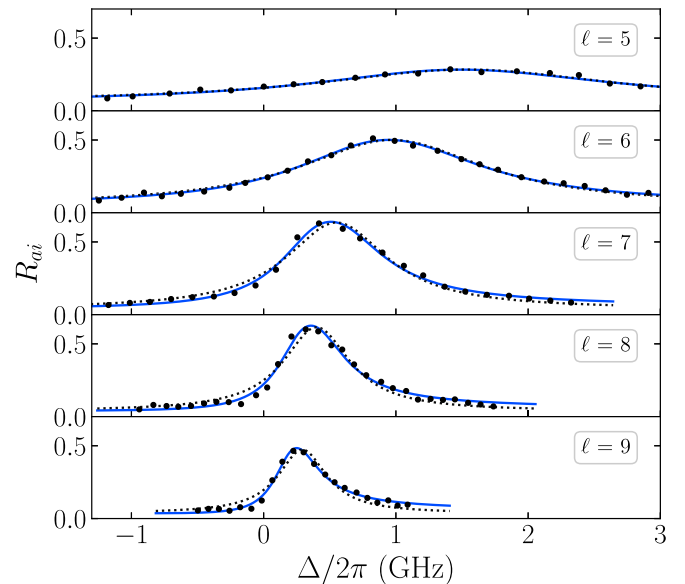

FIG. 3. Autoionization spectra at $n = 40$ for various ℓ, with a 3 μs ICE pulse duration. Δ is the detuning from the $6s_{1/2} \rightarrow 6p_{1/2}$ Yb$^+$ transition. Black circles: experimental points. Dashed gray lines: Lorentzian fits. Solid blue lines: fit with asymmetric $g(\Delta)$ function.
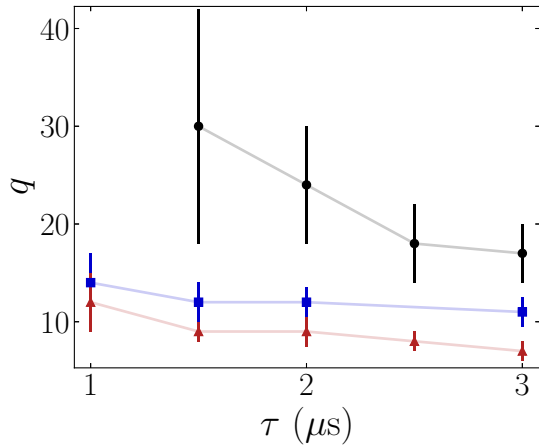
FIG. 4. Evolution of the asymmetry parameter q with ICE pulse duration τ for $\ell = 7$ (black circle), $\ell = 8$ (blue square), and $\ell = 9$ (red triangle). Error bars from the fit with asymmetric $g(\Delta)$ function.

FIG. 5. Autoionization linewidth Γ as a function of ICE pulse duration τ for $\ell = 7$ (black circle), $\ell = 8$ (blue square), and $\ell = 9$ (red triangle). Despite taking the depletion into account, we observe a dependence on the pulse duration which is linked to the appearance of asymmetry in the spectra. Error bars from the fit with asymmetric $g(\Delta)$ function.

The autoionization profile of doubly excited states is often explained by a quantum interference between two excitation paths: the ionization of the doubly excited state and the direct excitation of the continuum, leading to the so-called Fano profile [14] for the excitation cross section:

$$f(\Delta) = \frac{(q\Gamma/2 + \Delta - \Delta_0)^2}{\Gamma^2/4 + (\Delta - \Delta_0)^2}, \tag{1}$$

where Δ_0 is the energy shift compared to the energy of the doubly excited state, Γ is the autoionization rate, and q is a symmetry factor, with growing asymmetry for decreasing q. The q parameter is often proportional to the ratio of the excitation amplitudes of the doubly excited state and the continuum. As we produce a significant autoionized fraction, the cloud can become depleted, which appears as a saturation broadening depending on the pulse duration. The saturation can be modeled with the following fitting function:

$$g(\Delta) = \eta \left[1 - \exp \left(-\mu \Gamma \tau \frac{(q\Gamma/2 + \Delta - \Delta_0)^2}{\Gamma^2/4 + (\Delta - \Delta_0)^2} \right) \right], \tag{2}$$

where τ is the laser pulse length and μ is a fitted parameter proportional to the photon flux. Finally, we introduce an efficiency parameter η which accounts for the geometrical mismatch between the beam and the cloud and is fixed at the value 0.7.

However, in the case of the isolated core excitation of Rydberg states, the ICE laser is usually tuned well above the I_{6s} ionization limit and direct photoionization is then strongly reduced. In that case, the relevant processes are interferences between the excitation of the $6p_{1/2}n\ell$ state and the neighboring $6p_{1/2}n'\ell$ states [15]. For high ℓ states, the autoionization linewidth becomes much narrower than the energy difference to the $6p_{1/2}(n \pm 1)\ell$ states and the spectrum can be approximated by a simple "saturated" Lorentzian [10].

Nevertheless, an asymmetric shape can be seen for the higher ℓ states. In order to understand this feature, one can look at different pulse durations. In Fig. 4, we can see an increase of the asymmetry with the pulse duration, although it should be independent in the framework of Fano interfer-
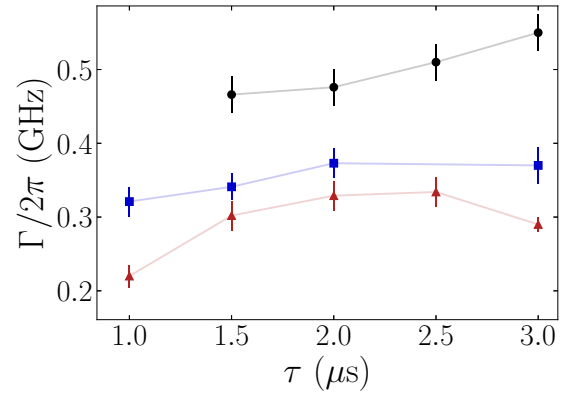
ences. This result discards a Fano-type phenomenon as an explanation for the asymmetry.

On the other hand, experimental biases such as local charge effects could explain these asymmetries in the spectra. Charges in the cloud, induced by Penning ionizations or autoionization of Rydberg atoms, will mix a fraction of $(\ell \pm 1)$ character in the $6s_{1/2}n\ell$ state from Stark effect, thus allowing transitions from $6s_{1/2}n\ell$ to $6p_{1/2}n(\ell \pm 1)$ states. The sudden appearance of the charges may also project the atoms into $6s_{1/2}n(\ell \pm 1)$ states [16], thus allowing transitions from $6s_{1/2}n(\ell \pm 1)$ to $6p_{1/2}n(\ell \pm 1)$ states. Finally, the corresponding Stark effect will shift all these transitions depending on the distance to the charge. The resulting spectrum can then reveal a strongly asymmetric profile. Considering our Rydberg atom density of about 10^7 cm^{-3}, these effects are likely to occur and should increase with the pulse duration due to an increasing number of charges. A more systematic study with smaller pulse durations and varying densities might enable one to determine exactly which of these effects are actually relevant. Nevertheless, in order to extract the linewidth and shift from the spectra, one cannot use the corresponding multiple sum of Lorentzians as the different peaks are not resolved and it would use too many fitting parameters. Therefore we decided to use the g function anyway, as introduced in Eq. (2), in the remainder of this article. This has the advantage of taking into account the depletion effect as well as the asymmetry in a simple function.

Using this fitting function, we extract the autoionization linewidths and the frequency shifts as a function of the pulse duration. The extracted linewidths are displayed in Fig. 5. One can see that the autoionization linewidth depends significantly on the pulse duration. Both the linewidth and the asymmetry increase with increasing pulse duration, and accurate autoionization rates can be obtained by extrapolating the curves towards a zero pulse duration. However, the behavior at small pulse duration is unclear and we prefer choosing the linewidth at the smallest measured pulse duration. We then estimate the error by taking the difference with the linewidth at twice this duration. We also add the fitting procedure uncertainty.
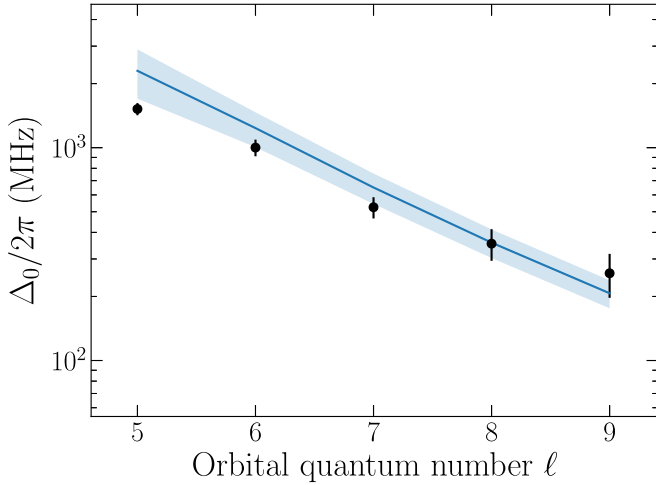
FIG. 6. Solid line: calculated energy shift of the ICE $6s_{1/2}40\ell \to 6p_{1/2}40\ell$ transition. The shaded area represents the range spanned by the possible values of the Yb$^+$ $\langle 6p_{1/2}|r^2|6p_{3/2}\rangle$ radial integral. Black points: measured energy shifts.

The experimental linewidths obtained are presented in Fig. 7 and compared to the theoretical predictions explained in next section. They are also summarized in Table I, together with the extracted shifts, which are presented in Fig. 6. Although the center frequency shifts hardly depend on the pulse duration, we applied the same procedure for their extraction. Another significant error for the center frequency shifts is the absolute uncertainty on the knowledge of the $6s_{1/2} \to 6p_{1/2}$ frequency of the ytterbium ion. This adds a 40 MHz error [13].
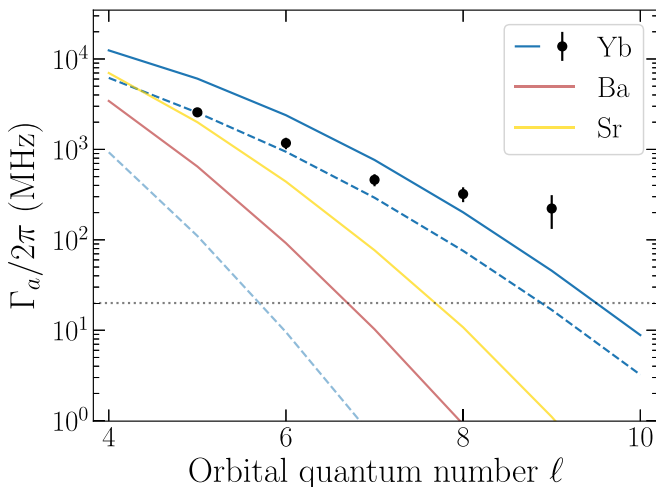

FIG. 7. Theoretical linewidths of the ICE spectrum $6s_{1/2}40\ell \to 6p_{1/2}40\ell$ for $K = \ell - 1/2$ (blue solid line) and $K = \ell + 1/2$ (dashed blue). We extract the largest ($K = \ell + 1/2$) of the two contributions of $6s_{1/2}\epsilon l$ (light-blue dashed lines) and see it is negligible. Comparison with the $6s_{1/2}40\ell \to 6p_{1/2}40\ell$ of barium (red) and the $5s_{1/2}40\ell \to 5p_{1/2}40\ell$ of strontium (yellow), both for $K = \ell + 1/2$. Black dots: experimental results for ytterbium. Dotted gray line: radiative linewidth for ytterbium of 20 MHz.

TABLE I. Experimental and theoretical results for the frequency shifts and linewidths for ICE of Yb on the $6s_{1/2}40\ell \to 6p_{1/2}40\ell$ transition s.

ℓ	Expt. shift (MHz)	Theor. shift (MHz)	Expt. width (MHz)	Theor. $K = \ell_2 - 1/2$,	width $\ell_2+1/2$
5	1520(100)	2297(600)	2570(170)	6062	2551
6	1001(90)	1236(230)	1175(170)	2389	942
7	525(60)	650(110)	461(70)	763	292
8	354(60)	358(55)	321(60)	201	76
9	257(60)	207(31)	220(90)	45	17

IV. THEORETICAL METHODS

Due to the weak overlap between the inner electron and the Rydberg one, high-ℓ Rydberg states of divalent atoms can be described using a perturbative approach, taking into account two-electron interactions in the frame of the $(j_1 - \ell_2)K$ coupling scheme where index 1 stands for the inner electron and index 2 stands for the Rydberg electron. We follow previous works performed on barium [10,17] and apply them to the case of ytterbium. We consider the following two-valence-electron Hamiltonian $H = H_1 + H_2 + H_I$ where H_1 is the independent inner electron Hamiltonian of the ^{174}Yb$^+$ ion. H_2 corresponds to the Rydberg electron Hamiltonian. The third term $H_I = 1/r_{12} - 1/r_2$ accounts for the interaction between the inner and outer electrons. We have performed our calculations with the following assumptions:

(1) The Rydberg electron radius r_2 is much larger than the inner electron radius r_1.

(2) High-ℓ Rydberg wave functions are approximated as hydrogenic wave functions.

In zero order, that is to say, neglecting the interaction Hamiltonian H_I, the energy is given by the sum of the two independent electron energies: $E^{(0)} = E_{n_1\ell_1 j_1} - 1/2n_2^2$. The interaction Hamiltonian is then introduced perturbatively. For that matter, we use a Taylor expansion of $1/r_{12}$ in terms of the tensorial operators associated with the spherical harmonics $C^{(q)}(\theta_i, \phi_i)$ [18].

Autoionization rates are calculated using the Fermi golden rule. From a $6p_{1/2}n\ell$ state, only four continua contribute to autoionization in first order: $6s_{1/2}\epsilon\ell \pm 1$ and $5d_{3/2}\epsilon\ell \pm 1$ where ϵ corresponds to the energy of the ejected electron. The autoionization rate then reads

$$\Gamma_{ai} = \sum_{\langle\epsilon|} \left| \langle \epsilon | \frac{r_1}{r_2^2} C_1^{(1)} C_2^{(1)} | 6p_{1/2} n_2 \ell_2 KM \rangle \right|^2, \quad (3)$$

where $\langle \epsilon |$ corresponds to the continua previously mentioned. All inner electron dipolar radial integrals were deduced from weighted oscillator strengths in [19], which was chosen for its completeness. The weighted oscillator strengths from $6p_{1/2}$ down to $6s_{1/2}$ and $5d_{3/2}$ are 0.465 and 0.126, respectively. We then find the reduced matrix elements $\langle 6s_{1/2} ||r|| 6p_{1/2}\rangle$ and $\langle 6p_{1/2} ||r|| 5d_{3/2}\rangle$ to be 2.38 and 3.18, respectively. Finally we deduce the radial integral to be 2.91 and 2.75 in atomic units, respectively. These values are similar to the ones in [20], and references therein. The Rydberg electron integrals are

found using the known analytical formula for hydrogen and continuum integrals were calculated with a standard Numerov technique [21].

In order to compute the transition energy shift, we compute the shift of both states $6s_{1/2}n_2\ell_2$ and $6p_{1/2}n_2\ell_2$ and take the difference. The first-order correction to the energy is null and the second-order correction to the energy of the $|n_1\ell_1 j_1 n_2\ell_2 KM\rangle$ state is expressed as

$$E^{(2,q)} = \sum_{q,|i\rangle} \frac{\left| \langle n_1\ell_1 j_1 n_2\ell_2 KM | \frac{r_1^q}{r_2^{q+1}} C_1^{(q)} C_2^{(q)} |i\rangle \right|^2}{E_{n_1 l_1 j_1} - E_i}, \quad (4)$$

where $|i\rangle = |n_1'\ell_1' j_1' n_2'\ell_2' K'M'\rangle$ is every state other than $|n_1\ell_1 j_1 n_2\ell_2 KM\rangle$ and $E_i = E_{n_1'\ell_1' j_1'}$ is the zeroth-order energy of this state. To simplify the sum of Eq. (4) we have made several approximations. We took into account the doubly excited states with ion cores for which an oscillator strength to either the Yb^+ $6s_{1/2}$ or $6p_{1/2}$ state is provided in [19] (21 and 14 states coupling to $6s_{1/2}$ and $6p_{1/2}$, respectively).

They correspond to a complete set of the lowest energy states, including states with an excited $4f$ shell $4f^{13}n_1\ell_1 n_2\ell_2$, and other higher levels induce a negligible energy shift. Quadrupolar ($q = 2$) interactions are typically an order of magnitude lower for $\ell = 5$ and vanish for largest orbital momenta so we ignore them, with one exception. We include the quadrupole coupling of $|6p_{1/2}40\ell_2\rangle$ to $|6p_{3/2}40\ell_2'\rangle$ which is particularly close in energy. The corresponding radial integral could not be found in literature but realistic boundaries from the reduced matrix elements $\langle 6p_{1/2}||r^2||6p_{1/2}\rangle = 32$ and $\langle 6p_{3/2}||r^2||6p_{3/2}\rangle = 51$ [22] can be deduced for the radial integral: $39.2 < \langle 6p|r^2|6p\rangle < 44.2$. Finally we use $41.7 \pm 5\%$. We also take a $\pm 5\%$ uncertainty on the dipolar terms [19] and consider a worst case scenario when summing uncertainties. In Fig. 6, we show our experimental extracted energy shifts compared to the theoretical shifts within these boundaries. We see good agreement between theoretical shifts and experimental ones. The residual difference with theory is probably explained by larger uncertainties in the oscillator strengths and missing quadratic terms.

V. DISCUSSION

Due to the relative complexity of the Stark excitation spectrum, we were not able to determine which of the two K states or if a linear combination of these two states was excited. Therefore, we plot in Fig. 7 the theoretical linewidth of both K states to compare to our results. We also plot the contribution to the total rate by autoionization to the two $|6s_{1/2}\epsilon\ell'\rangle$ continua. As shown by Fig. 7 the coupling to the other two continua $|5d_{3/2}\epsilon\ell'\rangle$ dominates the autoionization rate. Indeed, the small energy difference between the $5d_{3/2}$ and $6p_{1/2}$ states in the Yb^+ ionic core implies a larger overlap of the continuum wave function with the initial $6p_{1/2}n\ell$ wave function. Comparing to the case of barium and strontium, for which the energy difference between the corresponding $d_{3/2}$ and $p_{1/2}$ states is significantly higher, we find that the autoionization rates are indeed much lower. The experimental

results compare very well with the theoretical ones especially at low ℓ. At larger ℓ the growing mismatch is probably linked to the appearance of the asymmetry in the spectra. Another explanation, not explored here, is the possibility for the Rydberg electron to interact not with just one core electron but with two and couple to the ion core state $|4f^{13}(^2F_{7/2})5d6s(^3D), K = 3/2, J = 5/2\rangle$ at only around 9 THz below $|4f^{14}6p_{1/2}\rangle$.

We recall our motivation is to evaluate the feasibility of *nondestructive* imaging of Rydberg atoms by fluorescence of the IC. It is therefore necessary to reduce the autoionization rate below the radiative decay rate. Theoretically, one can see that this condition can be reached for $\ell \geqslant 10$ states for $n = 40$ states in ytterbium. However, as discussed above, those states are very sensitive to electric field and even a relatively low amount of charge in the cloud can affect the purity of the state. Consequently this imaging technique should probably be restricted to low densities. We also note that other atoms like barium or strontium are more favorable. Ultimately, it is preferable to choose circular states $n, \ell = n - 1, m = \ell$ which have the lowest Rydberg electron probability density close to the core, and have the slowest autoionization rates. Additionally, these states have the benefit of being insensitive to electric fields. Even though the creation of these states demands some effort [23], they are promising for an ICE-based imaging technique.

VI. CONCLUSION

In summary, we have investigated both experimentally and theoretically the isolated core excitation of ytterbium atoms in the high-orbital $6s40\ell$ Rydberg states with $\ell = 5$–9. The spectra obtained contained two main features: an unexpected asymmetry for the higher ℓ states, and a relatively low decrease of the linewidth when increasing ℓ. The analysis of the experimental spectra shows that asymmetry probably comes from charge-induced effects. A theoretical model based on perturbation theory has been used to compute the linewidth and the central energy shifts of the spectra. Due to a strong coupling between the $6p_{1/2}40\ell$ doubly excited level and the $5d_{3/2}\epsilon\ell'$ continua, the decrease of the linewidth with increasing ℓ is found to be relatively slow. This is in good agreement with the experimental measurements. These results lead us to the conclusion that with good control of the electric fields, a nonautoionizing state may be reachable for $\ell \geqslant 10$ at $n = 40$ and could allow an ICE-based fluorescence imaging. Although, circular states seems ultimately more promising for that application.

[1] H. Weimer, M. Müller, I. Lesanovsky, P. Zoller, and H. P. Büchler, Nat. Phys. **6**, 382 (2010).

[2] P. Schauss, M. Cheneau, M. Endres, F. Takeshi, S. Hild, A. Omran, T. Pohl, C. Gross, S. Kuhr, and I. Bloch, Nature (London) **491**, 87 (2012).

[3] H. Labuhn, D. Barredo, S. Ravets, S. de Leseleuc, T. Macri, T. Lahaye, and A. Browaeys, Nature (London) **534**, 667 (2016).

[4] H. Bernien, S. Schwartz, A. Keesling, H. Levine, A. Omran, H. Pichler, S. Choi, A. S. Zibrov, M. Endres, M. Greiner, V. Vuletic, and M. D. Lukin, Nature (London) **551**, 579 (2017).

[5] S. de Léséleuc, V. Lienhard, P. Scholl, D. Barredo, S. Weber, N. Lang, H. P. Büchler, T. Lahaye, and A. Browaeys, Science **365**, 775 (2019).

[6] W. E. Cooke, T. F. Gallagher, S. A. Edelstein, and R. M. Hill, Phys. Rev. Lett. **40**, 178 (1978).

[7] P. McQuillen, X. Zhang, T. Strickler, F. B. Dunning, and T. C. Killian, Phys. Rev. A **87**, 013407 (2013).

[8] G. Lochead, D. Boddy, D. P. Sadler, C. S. Adams, and M. P. A. Jones, Phys. Rev. A **87**, 053409 (2013).

[9] G. Fields, X. Zhang, F. B. Dunning, S. Yoshida, and J. Burgdörfer, Phys. Rev. A **97**, 013429 (2018).

[10] R. R. Jones and T. F. Gallagher, Phys. Rev. A **38**, 2846 (1988).

[11] R. R. Freeman and D. Kleppner, Phys. Rev. A **14**, 1614 (1976).

[12] J. J. McLoughlin, A. H. Nizamani, J. D. Siverns, R. C. Sterling, M. D. Hughes, B. Lekitsch, B. Stein, S. Weidt, and W. K. Hensinger, Phys. Rev. A **83**, 013406 (2011).

[13] I. Zalivako, I. Semerikov, A. Borisenko, V. Smirnov, P. Vishnyakov, M. Aksenov, P. Sidorov, N. Kolachevsky, and K. Khabarova, J. Russ. Laser Res. **40**, 375 (2019).

[14] U. Fano, Phys. Rev. **124**, 1866 (1961).

[15] N. H. Tran, R. Kachru, and T. F. Gallagher, Phys. Rev. A **26**, 3016 (1982).

[16] J. Millen, G. Lochead, and M. P. A. Jones, Phys. Rev. Lett. **105**, 213004 (2010).

[17] L. Pruvost, P. Camus, J. M. Lecomte, C. R. Mahon, and P. Pillet, J. Phys. B: At., Mol. Opt. Phys. **24**, 4723 (1991).

[18] B. Judd, *Operator Techniques in Atomic Spectroscopy*, (Princeton University Press, Princeton, NJ, 1963).

[19] B. Fawcett and M. Wilson, At. Data Nucl. Data Tables **47**, 241 (1991).

[20] S. G. Porsev, M. S. Safronova, and M. G. Kozlov, Phys. Rev. A **86**, 022504 (2012).

[21] M. L. Zimmerman, M. G. Littman, M. M. Kash, and D. Kleppner, Phys. Rev. A **20**, 2251 (1979).

[22] M. S. Safronova (private communication).

[23] P. Nussenzveig, F. Bernardot, M. Brune, J. Hare, J. M. Raimond, S. Haroche, and W. Gawlik, Phys. Rev. A **48**, 3991 (1993).